

# The Curriculum Is the Mechanism: Dissecting COCONUT’s Latent Thought Gains on ProsQA

Anonymous Author(s)

Anonymous Institution

**Abstract.** COCONUT’s training curriculum has not been isolated from its recycling mechanism. We construct a factorial control design: M4 matches COCONUT’s sequential multi-pass processing but uses fixed embeddings instead of recycled hidden states; M3 uses the same fixed embeddings in a single forward pass. M3 reaches 96.6% test accuracy (McNemar  $p = 0.845$  vs. COCONUT’s 97.0%); M4 reaches 94.8%. Three converging experiments — corruption analysis, linear probing, and cross-model transplantation — fail to distinguish COCONUT from M3 on any diagnostic where sequential reasoning and curriculum-driven computation make divergent predictions. The factorial decomposition reveals that recycled content impairs chain-length extrapolation (M4 outperforms COCONUT by 10.9pp on 7-hop,  $p < 0.001$ ), while sequential processing drives topological generalization (M4 outperforms M3 by 7.9pp on DAG,  $p < 0.001$ ). Recycled content also produces higher confidence that becomes miscalibrated on extended chains. At GPT-2 124M scale, the training curriculum — not the continuous thought mechanism — drives COCONUT’s accuracy on ProsQA.

## 1 Introduction

Chain-of-thought prompting shows that large language models solve multi-step reasoning more reliably when they externalize intermediate steps (Wei et al., 2022), raising the question of whether explicit verbalization is necessary. COCONUT (Hao et al., 2024) offers the most direct test: it replaces chain-of-thought tokens with continuous thought tokens, recycling the transformer’s final-layer hidden state back into the input stream across multiple positions. On ProsQA, a synthetic graph-traversal task, COCONUT achieves 97% accuracy, substantially outperforming chain-of-thought baselines (~80%). The authors attribute this gain to the expressiveness of the continuous latent space.

This attribution faces an uncontrolled confound. COCONUT is trained with a 7-stage curriculum that progressively removes explicit reasoning tokens, forcing the model to internalize computation that was previously externalized. The curriculum transforms the training distribution, the loss landscape, and the model’s learned representations simultaneously with the introduction of the recycling mechanism. Any performance gain could arise from the curriculum alone, from the mechanism alone, or from their interaction. Prior work by Deng et al. (2024) has shown that progressive removal of chain-of-thought steps can teach models implicit reasoning, suggesting the curriculum may be the active ingredient. Without a control that isolates one factor from the other, the causal claim remains underdetermined.

We introduce two curriculum-matched pause-token controls: M3 replaces recycled hidden states with a fixed learned embedding in a single forward pass; M4 matches

COCONUT’s sequential multi-pass processing while retaining the fixed embedding, enabling a clean factorial decomposition of recycled content and sequential processing (Section 3.2). M3 matches COCONUT on in-distribution ProsQA; three converging experiments fail to distinguish the two models on any diagnostic where sequential reasoning and curriculum-driven computation make divergent predictions. On out-of-distribution tests, the factorial decomposition reveals that recycled content impairs chain-length extrapolation while sequential processing drives topological generalization, and that recycled content produces miscalibrated confidence on extended chains.

This paper makes three contributions. First, we introduce a factorial control methodology — single-pass and multi-pass pause-token baselines — that isolates the curriculum from the mechanism and decomposes out-of-distribution generalization into recycled-content and sequential-processing components. Second, we provide converging evidence from three independent experimental paradigms that the continuous latent mechanism is not the causal source of COCONUT’s in-distribution performance. Third, we show that recycled content produces systematically miscalibrated confidence on out-of-distribution chains — higher confidence with lower accuracy — revealing a failure mode specific to the recycling mechanism.

## 2 Related Work

**Chain-of-thought and latent reasoning.** Wei et al. (2022) established that intermediate reasoning steps substantially improve multi-step performance, raising the question of whether verbalization is necessary.

Several architectures move reasoning into latent space: Quiet-STaR (Zelikman et al., 2024) generates internal rationales at every token position, while Deng et al. (2024) showed that progressive removal of chain-of-thought steps can teach implicit reasoning — suggesting the curriculum, rather than any particular mechanism, may be the key ingredient.

**COCONUT and continuous thought.** Hao et al. (2024) proposed COCONUT, recycling the transformer’s last-hidden-state output back into the embedding stream and achieving 97% on ProsQA with a multi-stage curriculum. Zhu et al. (2025) proved continuous thought tokens are strictly more expressive than discrete chain-of-thought under certain conditions. Zhang et al. (2025) challenged the empirical picture through causal interventions on LLaMA 7B and 8B, finding COCONUT’s latent tokens are largely causally inert. Our work complements Zhang et al. by constructing an explicit alternative — the pause baseline — that matches COCONUT’s training regime while eliminating the recycling mechanism.

**Pause tokens and extra computation.** Goyal et al. (2024) showed that appending learned non-informative pause tokens improves performance on tasks benefiting from additional depth. The pause-token framework provides a natural control for COCONUT: if gains come from extra computation rather than latent content, a pause model trained under the same curriculum should perform comparably. Our M3 instantiates this control. Pfau et al. (2024) proved that even meaningless filler tokens expand the class of solvable problems by increasing effective computation depth.

## 3 Methods

### 3.1 Task: ProsQA

ProsQA (Hao et al., 2024) is a synthetic graph-traversal benchmark where each sample presents inheritance rules over nonsense entities (e.g., “Alex is a jompus. Every jompus is a zhorpus.”), followed by a binary question whose answer requires traversing the implied entity graph across 3 to 6 hops. The dataset contains 17,886 training samples, 300 validation samples, and 500 test samples. ProsQA is COCONUT’s strongest-case task (~97% vs. ~80% for chain-of-thought).

To illustrate: given rules mapping Alex → jompus → zhorpus → brimpus, the model must traverse a 3-hop chain to answer “Is Alex a brimpus or a daxil?” The models differ in how they process these thought positions (Table 1, Section 3.2).

### 3.2 Models

We train four models, all initialized from the same pretrained GPT-2 124M checkpoint (Radford et al., 2019; 124M parameters, 12 transformer layers, 768-dimensional hidden states). Table 1 summarizes the model configurations.

**Table 1:** Model configurations. All share the same pretrained initialization, optimizer, and hyperparameters. M2, M3, and M4 share the same curriculum schedule; M1 uses standard supervised training without curriculum stages.

| Model   | Thought mechanism   | Processing          | Curriculum                      |
|---|---|---------------------|---------------------------------|
| M1<br>(CoT)                                     | None — explicit text reasoning tokens                                 | Single pass         | No stages (standard supervised) |
| M2<br>(CO-CONUT)                                | Hidden states from previous pass recycled as input embeddings         | 6 sequential passes | 7-stage progressive CoT removal |
| M3<br>(Pause)                                   | Fixed learned pause embedding (nn.Parameter) at each thought position | Single pass         | Same 7-stage curriculum as M2   |
| M4<br>(Pause-embedding Multipass)(nn.Parameter) | Fixed learned pause embedding (nn.Parameter) at each thought position | 6 sequential passes | Same 7-stage curriculum as M2   |

M3 is the primary control: it shares every architectural and training detail with M2 (Table 1), differing only in what occupies thought positions — a fixed learned embedding rather than recycled hidden states.

However, M2 and M3 differ in two confounded ways: (1) the *content* of thought-token embeddings (recycled hidden states vs. fixed pause vectors) and (2) the *sequential processing structure* (6-pass incremental decoding vs. single-pass parallel). M4 resolves this confound by matching M2’s sequential processing while using M3’s fixed embeddings, creating a clean factorial decomposition:

- **M2 vs. M4:** Same sequential processing, different content → isolates recycled content
- **M3 vs. M4:** Same fixed content, different processing → isolates sequential processing
- **M2 vs. M3:** Both factors differ → confounded (for reference only)

If M4 matches M2, the sequential processing structure drives differences and recycled content is inert. If M4 matches M3, the single-pass architecture is sufficient and

M2’s advantages arise from recycled content. If M4 falls between, both factors contribute. Implementation details are in Appendix A.1.

### 3.3 Training

All models were trained for 50 epochs on the ProsQA training set (17,886 samples) with the hyperparameters in Table 1 (fp32 precision, seed 0). For the curriculum models (M2, M3, M4), training proceeds through 7 stages: Stage 0 (epochs 0–4) trains with full chain-of-thought supervision; at each subsequent stage  $k$ , the last  $k$  reasoning steps are replaced with thought tokens. By Stage 6 (epochs 30–49), all reasoning steps are latent. Thought positions are padded to 6 regardless of path length. Additional training details (hardware, per-model wall time, optimizer protocol) are in Appendix A.2.

### 3.4 Experiments

We design three experiments. Experiment 1 (corruption ablation) progressively replaces thought-token representations with calibrated Gaussian noise. Experiment 2 (representation probing) trains linear probes on frozen hidden states across a  $13 \times 6$  (layer  $\times$  position) grid. Experiment 3 evaluates out-of-distribution generalization on four test sets (7-hop, 8-hop, DAG, dense; 1,000 samples each). Experiments 1 and 2 are restricted to M2 and M3 due to M4’s KV-cache extraction incompatibility (Appendix A.1). A fourth analysis extracts teacher-forced log-probabilities by force-decoding through the answer prefix and measuring  $\log P(\text{species\_token})$ , testing for confidence differences via Wilcoxon signed-rank tests (Bonferroni-corrected  $k = 5$ ). Full methodological details are in Appendix A.3.

## 4 Results

### 4.1 Training Replication

Table 2 reports accuracy for all four models. M2 (CO-CONUT) achieves 97.0% test accuracy, replicating Hao et al. (2024). M3 (pause) reaches 96.6%, not significantly different from M2 (McNemar  $p = 0.845$ , 95% CI  $[-2.4, +1.6]\text{pp}$ , 26 discordant pairs: 14 M2-only correct, 12 M3-only correct). M4 (pause-multipass) reaches 94.8%; the 2.2pp gap from M2 does not reach significance after Bonferroni correction ( $p = 0.071$ ,  $p_{\text{Bonf}} = 0.354$ , 31 discordant pairs). M4 and M3 likewise do not differ significantly ( $-1.8\text{pp}$ ,  $p_{\text{Bonf}} = 0.680$ ).

**Table 2:** Accuracy by model on ProsQA validation ( $n = 300$ ) and test ( $n = 500$ ) sets. Test accuracy is from the independent experiment inference pipeline used throughout; see Appendix A.2 for the minor discrepancy with training-time evaluation.

M4’s best epoch (30) is 13–19 epochs earlier than

| Model                         | Mechanism                 | Processing          | Val Accuracy | Test Accuracy | Best Epoch |
|-------------------------------|---------------------------|---------------------|--------------|---------------|------------|
| M1<br>(CoT)                   | Explicit chain-of-thought | Single pass         | 79.67%       | 83.0%         | 44         |
| M2<br>(CO-CONUT)              | Hidden-state recycling    | 6 sequential passes | 97.3%        | 97.0%         | 49         |
| M3<br>(Pause)                 | Learned embeddings        | Single pass         | 97.3%        | 96.6%         | 43         |
| M4<br>(Pause-pause Multipass) | Learned embeddings        | 6 sequential passes | 96.7%        | 94.8%         | 30         |

M2 (49) and M3 (43); the 2.2pp gap does not reach significance after Bonferroni correction ( $p = 0.354$ ), though non-significance does not establish equivalence (Section 6). Detailed M4 plateau analysis is in Appendix A.2. M4’s validation accuracy plateaus near 95% from epoch 30 onward, fluctuating between 93.7% and 96.7% through epoch 49 (Appendix A.2), suggesting the gap reflects architectural capacity limits rather than insufficient training.

### 4.2 Experiment 1: Corruption Ablation

M2 and M3 exhibit nearly identical degradation profiles under progressive forward corruption (Table A1 in Appendix A.5): accuracy remains near ceiling through position 3, drops precipitously between positions 3 and 4 (from  $\sim 96\%$  to  $\sim 57\%$ ), and collapses to near chance by position 6, with a maximum difference of 1.0pp at any corruption level. Single-position corruption confirms that position 3 alone is critical (M2: 57.6%, M3: 57.8%), ruling out redundant distributed storage (Appendix A.8). Permutation testing (5,000 trials per model) produced zero prediction flips (excludes true flip rate  $> 0.06\%$  at 95% confidence). Cross-problem transplantation succeeded for both models (M2: 97.0%, M3: 96.5% with hop-count-matched donors), confirming thought representations carry no problem-specific information (Appendices A.6–A.7).

### 4.3 Experiment 2: Representation Probing

Linear probes trained on frozen hidden states reveal that both models concentrate step-specific encoding at thought position 3 with near-identical selectivity profiles (Table 3; full selectivity data in Figure 3, Appendix A.4). At position 3 ( $n = 298$ ), selectivity reaches +52.0pp for M2 and +52.3pp for M3 — a 0.3pp difference

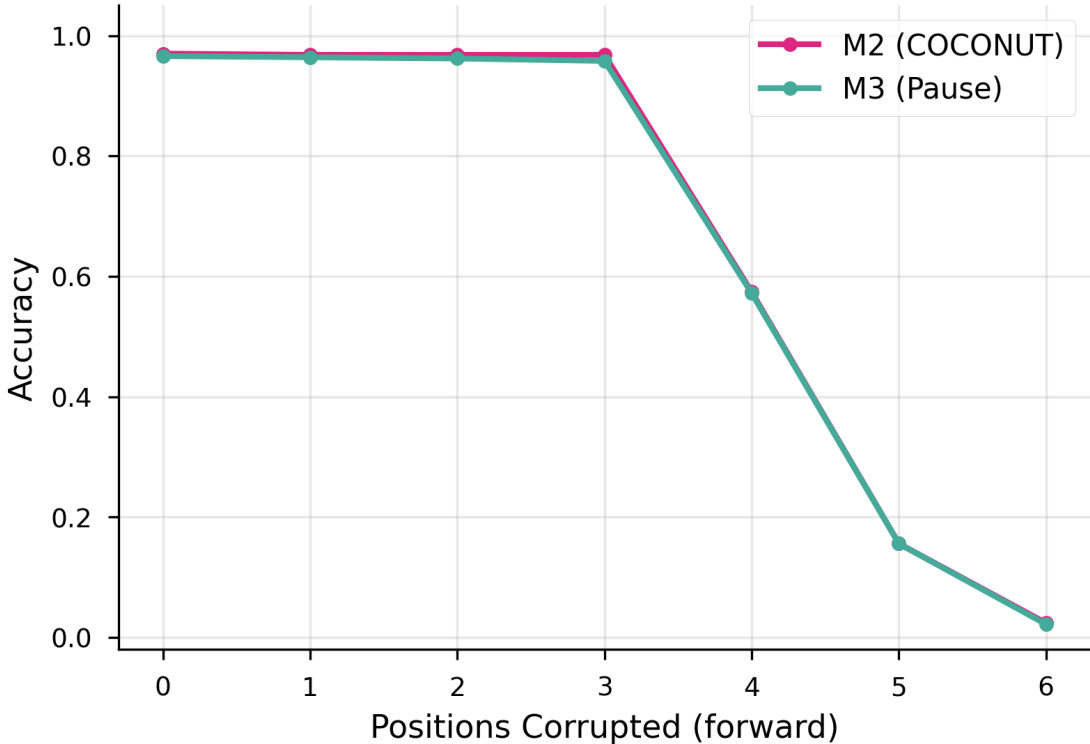


**Figure 1:** Progressive forward corruption accuracy for M2 (COCONUT) and M3 (Pause). Both models degrade identically, with a cliff between positions 3 and 4.

within cross-validation variability. Positions 0 and 1 are anti-selective in both models, indicating both broadcast answer-relevant information to early positions rather than constructing a sequential chain.

**Table 3:** Probing summary statistics for M2 and M3. Selectivity computed per-position using corrected sample sizes (see Appendix A.4). Full probe grids in Appendix A.9; nonlinear probe results in Appendix A.10.

| Metric                          | M2               | M3               |
|---------------------------------|------------------|------------------|
| Peak probe accuracy             | 55.4%            | 57.0%            |
| Peak location (layer, position) | (0, 3)           | (12, 3)          |
| Position 3 selectivity          | +52.0pp          | +52.3pp          |
| Positions 0–1 selectivity       | −15.6pp, −10.6pp | −12.0pp, −14.6pp |
| Significant cells (Bonferroni)  | 29 / 78          | 11 / 78          |

M2 shows broader probing signal (29/78 significant cells vs. 11/78) and higher thought-vs-input advantage (10.5% vs. 4.0%), but this richer encoding does not translate to an accuracy advantage (Section 4.4). Full heatmaps and nonlinear analysis are in Appendices A.10–A.11.

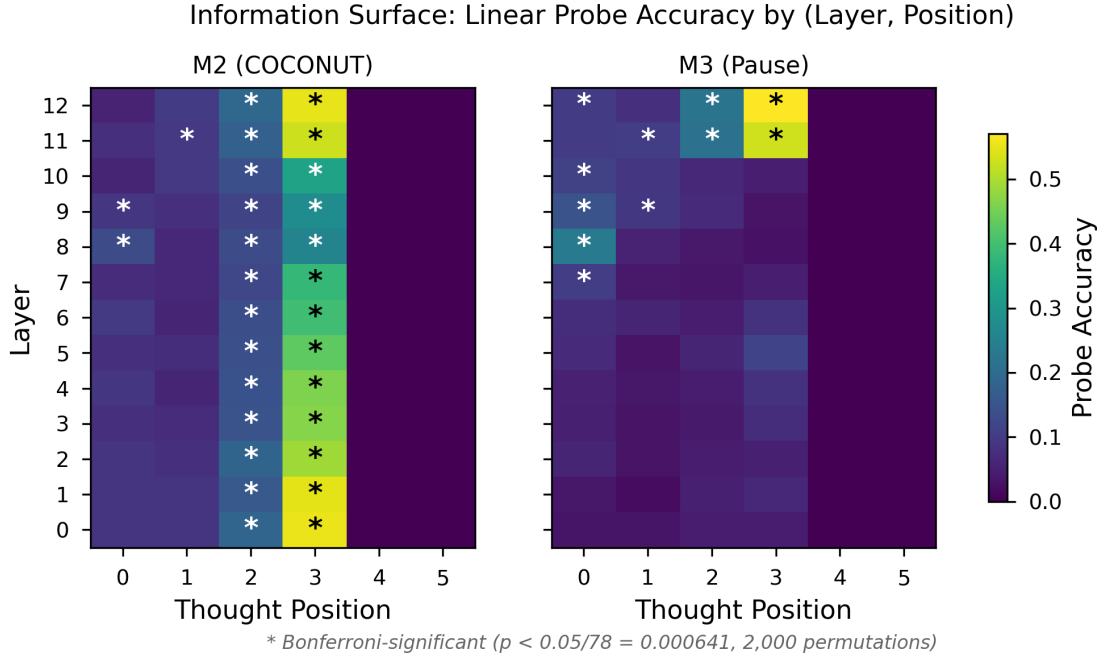
#### 4.4 Experiment 3: Out-of-Distribution Generalization

Table 4 reports OOD accuracy for all models. The confounded M2 vs. M3 comparison shows task-dependent tradeoffs (pairwise details in Appendix A.12); the factorial decomposition via M4 separates the underlying factors (Table 5).

**Table 4:** Out-of-distribution accuracy for all models.

| Test Set    | n    | M2       |            |            |                      |
|-------------|------|----------|------------|------------|----------------------|
|             |      | M1 (CoT) | (CO-CONUT) | M3 (Pause) | M4 (Pause-Multipass) |
| ProsQA (ID) | 500  | 83.0%    | 97.0%      | 96.6%      | 94.8%                |
| 7-hop       | 1000 | 10.7%    | 66.0%      | 75.4%      | 76.9%                |
| 8-hop       | 1000 | 8.2%     | 67.5%      | 75.1%      | 75.2%                |
| DAG         | 1000 | 28.2%    | 59.2%      | 51.9%      | 59.8%                |
| Dense       | 1000 | 14.1%    | 61.2%      | 68.4%      | 64.8%                |

The factorial decomposition via M4 separates the two confounded factors (Table 5). Recycled content impairs chain-length extrapolation: M4 outperforms M2 by 10.9pp on 7-hop and 7.7pp on 8-hop (both  $p < 0.001$ ), with no significant difference on DAG or dense. Sequential processing helps topological generalization:



**Figure 2:** Linear probe accuracy by layer and thought position for M2 (left) and M3 (right). Stars indicate Bonferroni-significant cells ( $p < 0.05/78$ , 2,000 permutations).

M4 outperforms M3 by 7.9pp on DAG ( $p < 0.001$ ), with no significant difference on other tests.

**Table 5:** Factorial decomposition. M4 vs. M2 isolates recycled content; M4 vs. M3 isolates sequential processing.

| Test Set | M4    |     |       | M4    |     |      | p<br>(Bonf.)Sig. |       |       |     |
|----------|-------|-----|-------|-------|-----|------|------------------|-------|-------|-----|
|          | –     | b   | c     | –     | b   | c    |                  |       |       |     |
| M2       | 10    | 21  | 0.354 | No    | –   | 10   | 19               | 0.680 | No    |     |
| (ID)     | 2.2   |     |       |       | 1.8 |      |                  |       |       |     |
|          | pp    |     |       |       | pp  |      |                  |       |       |     |
| 7-       | +10.9 | 222 | 113   | <     | Yes | +1.5 | 139              | 124   | 1.000 | No  |
| hop      | pp    |     |       | 0.001 |     | pp   |                  |       |       |     |
| 8-       | +7.7  | 188 | 111   | <     | Yes | +0.1 | 141              | 140   | 1.000 | No  |
| hop      | pp    |     |       | 0.001 |     | pp   |                  |       |       |     |
| DAG      | +0.6  | 182 | 176   | 1.000 | No  | +7.9 | 235              | 156   | <     | Yes |
|          | pp    |     |       |       |     | pp   |                  |       | 0.001 |     |
| Dense    | +3.6  | 186 | 150   | 0.280 | No  | –    | 157              | 193   | 0.306 | No  |
|          | pp    |     |       | 3.6   |     | pp   |                  |       |       |     |

$b$  = number of samples where only the row model is correct;  $c$  = number where only the column comparator is correct. Exact binomial test (two-sided) on discordant pairs with Bonferroni correction ( $k = 5$ ).

The two factors combine approximately additively (detailed decomposition in Appendix A.13). M1 performs

near chance on all OOD sets (8–28%), confirming that curriculum-trained latent reasoning provides substantial generalization benefits over explicit chain-of-thought at this scale.

#### 4.5 Teacher-Forced Confidence Analysis

Teacher-forced log-probabilities reveal systematic confidence differences invisible to binary accuracy tests (M3 vs. M4 details in Appendix A.15).

On ProsQA, M2 assigns higher confidence than M4, but both achieve near-ceiling median probabilities (>99.9%); the difference is statistically large ( $r = 0.678$ ) but practically negligible. On OOD chain-length tasks, this confidence signal becomes miscalibrated: M2 is more confident yet less accurate than M4 on both 7-hop and 8-hop (full statistics in Table 6a, Appendix A.14). A mechanistic account of this miscalibration is discussed in Section 5.2. The confounded M2 vs. M3 comparison is in Appendix A.14.

Across all four results sections, a consistent pattern emerges: every diagnostic where sequential reasoning and curriculum-driven computation make divergent predictions favors the curriculum account. Section 5.1 synthesizes this convergent evidence.

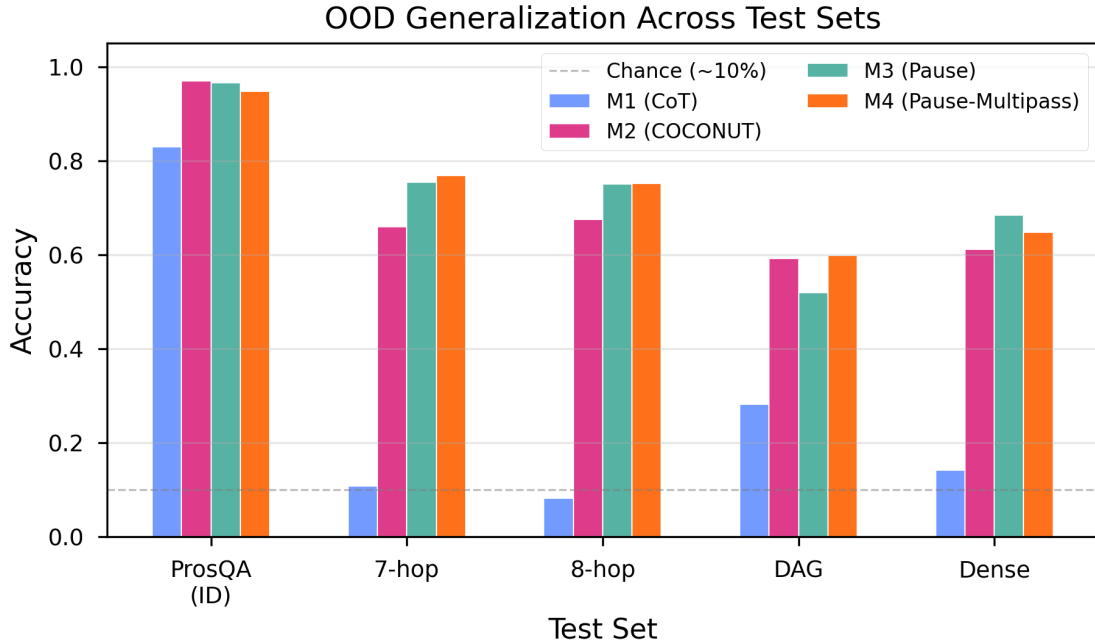


**Figure 3:** Out-of-distribution accuracy for M1, M2, M3, and M4 across four test sets.

## 5 Discussion

### 5.1 Convergent Evidence and Curriculum-Driven Representations

Seven independent diagnostics — permutation, transplant, corruption, selectivity, significance, OOD, and confidence — consistently favor the curriculum account over the sequential reasoning account (full analysis in Table A9, Appendix A.13). No single experiment is decisive: permutation insensitivity could reflect redundant encoding — if thought tokens encoded a sequential reasoning chain, reordering them should disrupt the dependency structure; the zero flip rate indicates that the model routes information by content rather than position — but single-position corruption rules this out — corrupting position 3 alone collapses accuracy to  $\sim 57\%$ , indicating concentrated rather than redundant storage. The identical cliff profiles rule out the possibility that M2’s recycled hidden states provide a more robust or differently structured representation than M3’s fixed embeddings — under matched perturbation, both models fail at exactly the same point. Both models encode step-specific information in identical patterns (+52pp selectivity at position 3), and this shared pattern arises from the curriculum that both models undergo, not from the recycling mechanism that only M2 possesses. M2’s richer encoding — 29/78 significant probing cells versus 11/78 — does not produce a detectable accuracy advantage. This dissociation between representational

richness and behavioral outcome is consistent with Ravichander et al. (2021): information linearly decodable from representations is not necessarily used by downstream computation.

### 5.2 Factorial Decomposition of OOD Performance

The factorial decomposition fully resolves the M2–M3 OOD tradeoff. M2’s chain-length disadvantage arises entirely from recycled content (M4 matches M3, not M2), while M2’s DAG advantage arises entirely from sequential processing (M4 matches M2, not M3). The factors combine additively and affect different task types. The recycled hidden states are not merely inert — on chain-length extrapolation, models trained with recycling generalize significantly worse than matched controls, possibly because recycled content carries distribution-specific information that becomes misleading at longer path lengths.

The teacher-forced confidence analysis supports this interpretation: during curriculum training on 3–6 hop problems, recycled content learns a confidence signal correlated with correctness; on out-of-distribution chains (7–8 hops), this signal persists even though the reasoning path exceeds the model’s capacity. Fixed embeddings avoid this failure mode because they carry no distribution-specific content.

### 5.3 Relation to Prior Work and Practical Implications

Our results extend Zhang et al.’s (2025) finding of causal inertness to ProsQA — COCONUT’s strongest-case task — strengthening generality across tasks and scales (GPT-2 124M through LLaMA 8B). Zhu et al.’s (2025) theoretical expressiveness is not realized in practice at this scale. Goyal et al.’s (2024) pause-token finding is confirmed and extended: curriculum-trained pause tokens match COCONUT in-distribution and exceed it on most OOD tests. For researchers building on COCONUT, curriculum design is likely the higher-return lever: the continuous thought mechanism roughly doubles VRAM consumption yet yields no measurable accuracy benefit at this scale.

## 6 Limitations

All experiments use GPT-2 124M on synthetic ProsQA with a single training seed. The continuous thought mechanism may provide benefits at larger scale or on tasks with ambiguous reasoning paths (Section A.16). M4’s 2.2pp gap from M2, though non-significant, may reflect a systematic architectural limitation; multi-seed replication would clarify. M4’s corruption and probing coverage is limited by KV-cache incompatibility (Appendix A.1). We do not test a curriculum-only condition (no thought positions), which would distinguish whether the curriculum alone drives gains or requires additional attention positions as computational budget. Extended discussion of each limitation is in Appendix A.16.

**Null-result sensitivity.** The convergent evidence in Section 5.1 chains multiple null or near-null diagnostics. Each has finite resolution: the permutation test (5,000 trials, 0 flips) excludes true flip rates above 0.06% at 95% confidence but cannot detect subtler ordering effects; the corruption analysis detects degradation differences of approximately 1 percentage point at  $n = 500$  (the maximum observed M2–M3 difference at any corruption level); the probing selectivity comparison (+52.0pp vs. +52.3pp) has cross-validation variability of approximately 2–3pp at  $n = 298$ , sufficient to detect a 5pp selectivity difference but not a 1pp difference. These bounds define the resolution of the null results: effects smaller than these thresholds would not be detected by the current experimental design.

## 7 Conclusion

A curriculum-matched pause baseline (M3) matches COCONUT on in-distribution ProsQA (McNemar  $p = 0.845$ ) and three converging experiments fail to distinguish the models on any diagnostic where sequential reasoning and curriculum-driven computation make

divergent predictions. The factorial decomposition via M4 resolves the out-of-distribution attribution: recycled content impairs chain-length extrapolation while sequential processing drives topological generalization.

At GPT-2 124M scale, the training curriculum drives COCONUT’s accuracy on ProsQA. The continuous thought mechanism affects internal representations and produces higher confidence that is practically negligible on in-distribution data (both models >99.9%) but becomes miscalibrated on extended chains; it does not improve accuracy. For researchers developing latent reasoning architectures, curriculum design warrants at least as much attention as the choice of thought-token mechanism. Code, configurations, and experiment scripts are available at [URL redacted for review].

## References

- Deng, Y., Yu, Y., Saha, S., Lu, J., & Hajishirzi, H. (2024). From explicit CoT to implicit CoT: Learning to internalize CoT step by step. *arXiv preprint arXiv:2405.14838*.
- Goyal, S., Didolkar, A., Ke, N. R., Blundell, C., Beaulieu, P., Mozer, M., Bengio, Y., & Ke, N. R. (2024). Think before you speak: Training language models with pause tokens. In *Proceedings of the Twelfth International Conference on Learning Representations (ICLR 2024)*.
- Hao, S., Gu, Y., Luo, H., Liu, T., Shao, L., Wang, X., Xie, S., Ma, T., Koltun, V., & Zettlemoyer, L. (2024). Training large language models to reason in a continuous latent space. *arXiv preprint arXiv:2412.06769*.
- Meng, K., Bau, D., Andonian, A., & Belinkov, Y. (2022). Locating and editing factual associations in GPT. In *Advances in Neural Information Processing Systems 35 (NeurIPS 2022)*.
- Pfau, J., Merrill, W., & Bowman, S. R. (2024). Let’s think dot by dot: Hidden computation in transformer language models. In *Findings of the Association for Computational Linguistics: ACL 2024*.
- Radford, A., Wu, J., Child, R., Luan, D., Amodei, D., & Sutskever, I. (2019). Language models are unsupervised multitask learners. *OpenAI Technical Report*.
- Ravichander, A., Belinkov, Y., & Hovy, E. (2021). Probing the probing paradigm: Does probing accuracy entail task relevance? In *Proceedings of the 16th Conference of the European Chapter of the Association for Computational Linguistics (EACL 2021)*, pp. 3363–3377.
- Saparov, A., & He, H. (2022). Language models are greedy reasoners: A systematic formal analysis of chain-of-thought. In *Proceedings of the Eleventh International Conference on Learning Representations (ICLR 2023)*.

Wei, J., Wang, X., Schuurmans, D., Bosma, M., Ichter, B., Xia, F., Chi, E., Le, Q., & Zhou, D. (2022). Chain-of-thought prompting elicits reasoning in large language models. In *Advances in Neural Information Processing Systems 35 (NeurIPS 2022)*.

Zelikman, E., Harik, G., Shao, Y., Jayasiri, V., Haber, N., & Goodman, N. D. (2024). Quiet-STaR: Language models can teach themselves to think before speaking. *arXiv preprint arXiv:2403.09629*.

Zhang, R., Du, Y., Sun, S., Guo, D., Liu, Z., Zheng, Q., & Li, L. (2025). On the causal role of continuous thought tokens. *arXiv preprint arXiv:2512.21711*.

Zhu, Z., Wang, T., & Dong, Y. (2025). On the expressiveness of continuous thought. In *Proceedings of the 42nd International Conference on Machine Learning (ICML 2025)*.

---

## Appendix

### A.1 Detailed Model Implementation

M3 was implemented by adding a `feedback_mode` parameter to the `Coconut` class in Meta’s official codebase. When `feedback_mode="continuous"` (default), the model operates as standard COCONUT (M2). When `feedback_mode="pause_curriculum"`, thought positions receive a learned `nn.Parameter` embedding and inference executes a single forward pass (M3). When `feedback_mode="pause_multipass"`, thought positions receive the same learned embedding but are processed sequentially across 6 passes, matching M2’s KV-cache incremental decoding structure (M4). The modification is minimal: a single branching parameter in the model class, with all other code (data loading, training loop, evaluation) shared across all models.

**FLOP comparison.** M3 requires substantially fewer inference-time FLOPs than M2. COCONUT’s recycling loop processes thought tokens sequentially: after a full forward pass over the input prefix, each subsequent thought token is processed as a single-token forward pass using KV-cache incremental decoding, with the previous position’s final-layer hidden state injected as the current position’s input embedding. M3 instead processes all thought tokens in a single forward pass alongside the input. M4 matches M2’s sequential processing structure exactly — processing thought tokens one at a time via KV-cache incremental decoding across 6 passes — but re-injects the same fixed pause embedding at each step rather than recycling content. M2 and M4 are matched on sequential processing structure and total FLOPs, differing only in what is injected at each step. M3 and

M4 differ only in whether thought tokens are processed sequentially or in parallel.

The only position-distinguishing signal available to M3 is GPT-2’s learned positional encoding; the pause embeddings carry no position-specific information. A key difference is that M2’s sequential KV-cache decoding restricts each thought position to attending only to preceding positions (causal mask over passes), whereas M3’s single-pass processing allows all thought positions to attend to each other simultaneously. M4 processes the same fixed embedding at each of its 6 sequential passes.

**M4 KV-cache incompatibility.** The corruption analysis and probing experiments extract hidden states by running a fresh forward pass on the model’s input embeddings, discarding the accumulated KV-cache state. For M2, whose continuous thought tokens are computed from recycled hidden states, this extraction correctly captures the model’s inference-time representations. For M4, the KV-cache accumulated across the 6 sequential passes IS the model’s computation — without it, extracted representations reflect only the fixed pause embedding processed in isolation, not the representation built through sequential accumulation. Corruption injection and probing on these artifacts would measure properties of the extraction pipeline, not of the model. The zero-corruption control confirms this: M4 produces chance-level accuracy (2.4%) under the extraction methodology even with no corruption applied.

### A.2 Training Details and Curves

**Hardware.** All training was conducted on a single NVIDIA H100 80GB GPU. M1 required approximately 8 hours; M2, M3, and M4 each required approximately 28–40 hours due to the multi-pass forward loop (M2, M4) and the longer sequences with thought tokens (all curriculum models). M4 is the slowest due to processing 6 sequential passes with fixed embeddings, which prevents the KV-cache optimization that COCONUT’s recycled states enable.

**Optimizer reset.** The optimizer was reset at the start of each epoch, following Meta’s training protocol (`reset_optimizer: True`). Training used the same matching configuration as Meta: batch size 32 with gradient accumulation over 4 steps on a single GPU, matching Meta’s original 4-GPU configuration of batch size 32 with no gradient accumulation.

**Inference pipeline discrepancy.** Training-time evaluation at best epoch yielded M2 = 98.0% and M3 = 95.6%, differing from the experiment pipeline by 5 samples per model in opposite directions. The discrepancy arises because the training-time evaluator (Meta’s `run.py`) and our experiment pipeline (`exp_ood.py`) differ in

tokenization handling of the answer prefix: the training evaluator conditions on teacher-forced prefix tokens, while the experiment pipeline uses greedy autoregressive decoding from the last thought token. We use the experiment-pipeline numbers throughout because all pairwise comparisons, corruption analyses, and OOD evaluations were conducted with the same pipeline, ensuring internal consistency.

**Training curves.** Figure 2 shows training curves for all four models across 50 epochs. M2, M3, and M4 converge at comparable rates under the shared curriculum schedule, while M1 plateaus earlier at a lower asymptote.

**M4 plateau analysis.** M4’s best epoch (30) occurs 13–19 epochs earlier than the other curriculum models (M2: 49, M3: 43, M1: 44). Inspection of M4’s full validation trajectory reveals that this early peak reflects noise in a high-variance plateau rather than overfitting: after epoch 30, validation accuracy fluctuates between 93.7% and 96.7% (matching the peak) for the remaining 20 epochs, with a second 96.7% hit at epoch 39. The “best epoch 30” selection captures a fluctuation peak in this plateau; the model’s late-training performance (epochs 30–49, mean ~95.0%) is stable but does not improve further. Two interpretations of this plateau are possible. First, M4’s multi-pass fixed-embedding architecture may converge to its representational capacity limit earlier than M2’s recycling architecture, which continues refining representations through epoch 49. Alternatively, our curriculum schedule — optimized for M2 — may be suboptimal for M4, leaving open the possibility that a longer or differently structured curriculum could unlock further gains. The present data cannot distinguish these accounts; dedicated M4 curriculum ablations would be needed to adjudicate.

### A.3 Detailed Experiment Methodology

**Experiment 1: Corruption Ablation — full predictions and conditions.** If thought tokens encode a sequential reasoning chain, three predictions follow: (a) corrupting early positions should cascade through the chain, producing gradual degradation proportional to the number of positions corrupted; (b) permuting the order of thought tokens should disrupt the sequential dependency, changing the model’s predictions; and (c) transplanting thought representations from one problem into another should fail, since a sequential chain encodes problem-specific intermediate states. If thought tokens instead serve as a generic compute buffer, the alternative predictions are: (a) degradation should be threshold-based — the model either has enough uncorrupted buffer positions to function or it does not; (b) permutation should have no effect, since buffer positions carry order-invariant information; and (c)

transplantation should succeed, since the buffer carries no problem-specific content.

We apply six corruption conditions:

- *Forward corruption*: progressively replace thought positions 0, 0:1, 0:2, ..., 0:5 with random embeddings drawn from a distribution matched to the model’s actual thought token statistics.
- *Reverse corruption*: the same procedure applied from the final position backward.
- *Single-position corruption*: replace only position  $k$  for each  $k$  in  $\{0, \dots, 5\}$ .
- *Permutation*: shuffle the order of the model’s own thought token hidden states for the same problem (10 random permutations per sample, 500 samples).
- *Partial permutation*: swap only adjacent pairs of thought tokens, testing sensitivity to local versus global ordering.
- *Cross-problem transplant*: inject thought representations from problem A into problem B (200 pairs, matched by hop count).

All random replacement embeddings were drawn to match the mean and standard deviation of each model’s actual thought token hidden states. For M2, this yielded an L2 distance of 202.65 from the originals. For M3, the L2 distance was 4.09. This 50-fold difference reflects the fundamental architectural distinction: recycled hidden states carry rich, variable information across problems, while pause embeddings are approximately constant. The per-model calibration ensures that each model’s corruption is scaled appropriately to its own activation magnitude, though the absolute perturbation sizes are not directly comparable between models.

**Experiment 2: Representation Probing — full methodology.** We extract hidden states at every (layer, thought position) cell in a  $13 \times 6$  grid (13 layers including the input embedding layer, 6 thought positions) and train linear probes (RidgeClassifier with default regularization) to classify the identity of the entity at the corresponding step in the ground-truth reasoning path. All probes use 5-fold cross-validation over 500 samples. The number of valid probe targets varies by position: all 500 samples contribute labels for positions 0–2, 298 for position 3, 81 for position 4, and 12 for position 5, reflecting the distribution of path lengths in the test set. Results for position 5 ( $n = 12$ ) should be interpreted with caution.

Three diagnostic metrics are computed. *Selectivity*: selectivity( $l, t$ ) =  $\text{probe\_acc}(\text{target} = \text{step}_t) - \max_{\{s \neq t\}} \text{probe\_acc}(\text{target} = \text{step}_s)$ . *Thought-minus-input advantage*: accuracy difference between probes on thought positions and input token positions. *Nonlinear probes*: 2-

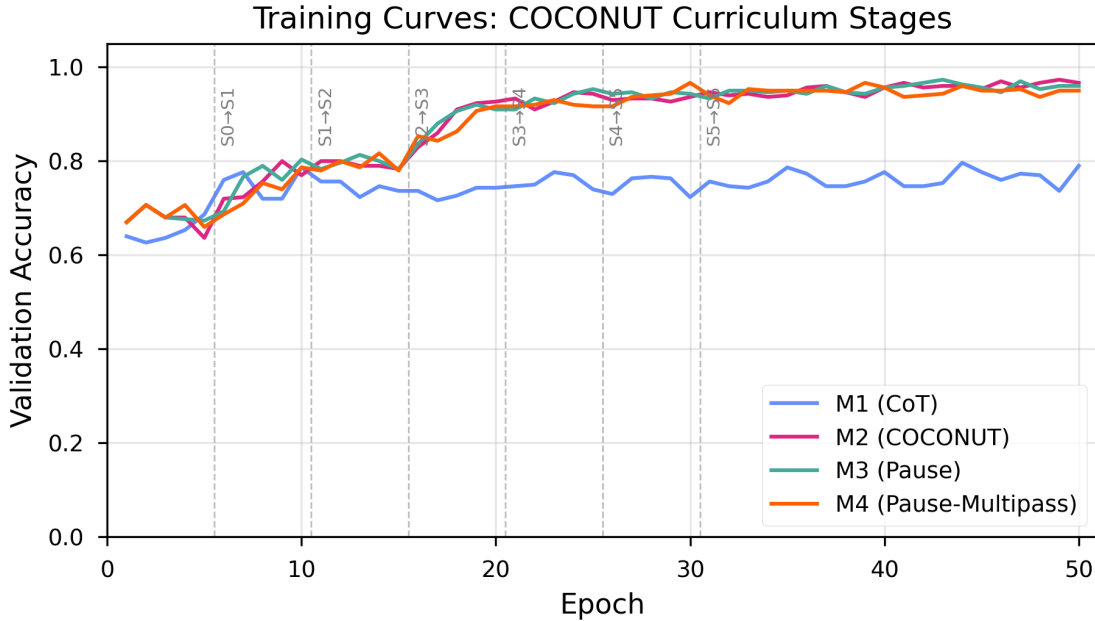


**Figure 4:** Training curves for M1 (CoT), M2 (COCONUT), M3 (Pause), and M4 (Pause-Multipass) across 50 epochs.

layer MLP probes with grid search over 72 hyperparameter configurations (6 hidden sizes  $\times$  3 learning rates  $\times$  4 regularization strengths; see Appendix A.10).

**Experiment 3: OOD — statistical methodology.** For statistical comparisons, we use exact McNemar’s test (two-sided binomial test on the disagreement counts) on each of the five test sets, applied to three pairwise comparisons: M2 vs. M3, M2 vs. M4, and M3 vs. M4. Bonferroni correction is applied within each comparison family. McNemar’s test uses only the discordant pairs (samples where exactly one model is correct) and is more powerful than marginal tests when agreement rates are high.

#### A.4 Selectivity Computation Correction and Corrected Permutation Tests

The original selectivity analysis truncated all positions to  $n = 12$  samples (limited by position 5), producing an artifactual selectivity of 0.0 across all cells. The corrected analysis uses each position’s full sample count (500 for positions 0–2, 298 for position 3, 81 for position 4). Position 5 ( $n = 12$ ) is excluded from quantitative claims. The corrected selectivity values are reported in Table 3 and Figure 3.

The same truncation invalidated the permutation-based significance tests computed during the original probing run: with only 12 samples across 38+ classes, probes returned near-zero accuracy regardless of label permutation, yielding uniformly non-significant p-values ( $p = 1.0$

for all 78 cells).

We reran permutation tests with corrected sample sizes using 2,000 permutations per cell (minimum achievable  $p = 1/2001 = 0.0005$ , below the Bonferroni threshold of  $0.05/78 = 0.000641$ ). The permutation test uses an optimized ridge classifier with precomputed Cholesky decomposition on a single 80/20 stratified split, counting exceedances with the conservative estimator  $p = (\text{count} + 1) / (\text{n\_perms} + 1)$ .

**M2 (COCONUT): 29/78 significant cells.** All 13 layers are significant at positions 2 and 3 (26 cells), plus layer 8 and 9 at position 0, and layer 11 at position 1. The peak accuracy of 55.4% at (layer 0, position 3) achieves  $p = 0.0005$ . Every layer at position 3 exceeds 25% accuracy (38-class chance = 2.6%), and every layer at position 2 exceeds 11.8%.

**M3 (Pause): 11/78 significant cells.** Significant cells are concentrated in late layers: layers 7–10 and 12 at position 0, layers 9 and 11 at position 1, layers 11–12 at position 2, and layers 11–12 at position 3. The peak accuracy of 57.0% at (layer 12, position 3) achieves  $p = 0.0005$ .

The key difference is in the distribution of significant cells. M2 shows significant probing accuracy across all layers at positions 2–3, consistent with the recycling mechanism injecting decodable information from the earliest layer. M3 shows significance only in late layers (primarily 9–12), consistent with representations being built through the transformer stack. This architectural

difference in where information is available does not produce a behavioral difference: both models achieve comparable task accuracy and selectivity profiles.

Positions 4 and 5 return 0.0% accuracy for both models ( $n = 81$  with 32 classes and  $n = 12$  with 12 classes, respectively); with more classes than the minimum fold size, stratified cross-validation cannot be computed, and these cells are excluded from significance testing.

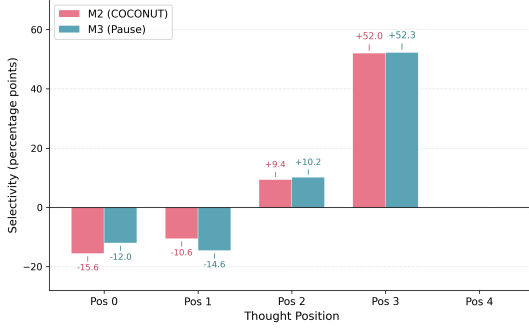


**Figure 5:** Step selectivity by thought position for M2 and M3. Both models show anti-selectivity at positions 0–1, mild selectivity at position 2, and strong selectivity at position 3 (+52.0pp and +52.3pp respectively).

## A.5 Cross-Corruption Results

**Table A1:** Progressive forward corruption under three noise conditions ( $n = 500$  per condition).

| Positions Corrupted | M2 + M2-noise (L2~203) | M3 + M3-noise (L2~4) | M3 + M2-noise (L2~203) |
|---------------------|------------------------|----------------------|------------------------|
| 0 (clean)           | 97.0%                  | 96.6%                | 96.6%                  |
| 1                   | 96.8%                  | 96.4%                | 96.6%                  |
| 2                   | 96.8%                  | 96.2%                | 96.4%                  |
| 3                   | 96.8%                  | 95.8%                | 96.4%                  |
| 4                   | 57.4%                  | 57.2%                | 57.6%                  |
| 5                   | 15.6%                  | 15.6%                | 15.8%                  |
| 6                   | 2.4%                   | 2.2%                 | 2.4%                   |

## A.6 Permutation Sensitivity and Power Analysis

**Permutation sensitivity.** We tested whether the ordering of thought tokens carries sequential information by permuting all latent positions and measuring the rate at which the model’s prediction changes. Across 500 test samples with 10 random permutations each (5,000 permutation trials per model), neither M2 nor M3 produced a single prediction flip (flip rate = 0.0%). Partial permutation experiments, in which subsets of positions were permuted, likewise produced a 0.0% flip rate. Both models treat thought positions as an unordered bag of compute with respect to final predictions. This does not rule

out order-sensitive internal representations that are ultimately redundant for the final prediction. This result creates a tension with the corruption findings: if individual positions carry no ordering information, yet corrupting position 3 alone collapses accuracy (Appendix A.8), the model must perform content-based routing — attending to what each position contains rather than where it falls in the sequence. The combination of order-invariance and position-specific criticality is consistent with an attention mechanism that selects the most informative position regardless of its index.

**Power analysis.** With 5,000 permutation trials and zero observed flips, the exact binomial test excludes a true flip rate above 0.06% at 95% confidence (0.09% at 99% confidence).

## A.7 Cross-Problem Transplantation

To test whether thought representations encode problem-specific information, we transplanted the full set of thought-token activations from one problem into another and measured accuracy on the recipient problem.

**Table A2:** Cross-problem transplantation accuracy under matched and unmatched conditions (200 pairs each).

| Condition                              | M2    | M3    |
|--|-------|-------|
| Clean (no transplant)                  | 97.0% | 96.6% |
| Matched transplant (hop-count aligned) | 97.0% | 96.5% |
| Unmatched transplant (random pairing)  | 97.5% | 96.5% |

Fully unmatched transplantation (random donor-recipient pairing with no hop-count matching) produced comparable results, confirming that thought representations carry no problem-specific or complexity-specific information.

## A.8 Full Corruption Results — Reverse and Single-Position

**Table A3:** Reverse corruption accuracy ( $n = 500$ ; corrupting from position 5 backward).

| Positions Corrupted | M2    | M3    |
|---------------------|-------|-------|
| 1 (pos 5)           | 97.0% | 96.6% |
| 2 (pos 4–5)         | 96.8% | 96.0% |
| 3 (pos 3–5)         | 96.8% | 96.0% |
| 4 (pos 2–5)         | 57.4% | 57.2% |
| 5 (pos 1–5)         | 15.6% | 15.4% |
| 6 (pos 0–5)         | 2.4%  | 2.2%  |

**Table A4:** Single-position corruption accuracy ( $n = 500$ ; corrupting only position k).

| Position Corrupted | M2    | M3    |
|--------------------|-------|-------|
| 0                  | 96.8% | 96.4% |
| 1                  | 96.8% | 96.2% |
| 2                  | 96.8% | 96.2% |
| 3                  | 57.6% | 57.8% |
| 4                  | 15.6% | 15.8% |
| 5                  | 2.4%  | 2.2%  |

Reverse and single-position corruption confirm the forward corruption findings. The cliff occurs at the same position regardless of corruption direction. Single-position corruption at position 3 alone causes the same catastrophic drop as corrupting positions 0–3 together, indicating that position 3 carries critical information while positions 0–2 carry mutually redundant copies of answer-relevant content.

*Figure reproduced in Section 4.2.*

## A.9 Full Linear Probe Accuracy Grids

**Table A5:** M2 (COCONUT) linear probe accuracy (%), 5-fold CV). Rows = transformer layers (0 = embedding layer, 12 = final layer). Columns = thought positions (0–5). Positions 4–5 show 0.0% due to insufficient samples ( $n = 81$  and  $n = 12$ ).

| Layer | Pos 0 | Pos 1 | Pos 2 | Pos 3 | Pos 4 | Pos 5 |
|-------|-------|-------|-------|-------|-------|-------|
| 0     | 8.6   | 8.6   | 18.6  | 55.4  | 0.0   | 0.0   |
| 1     | 8.8   | 8.8   | 16.0  | 54.7  | 0.0   | 0.0   |
| 2     | 8.8   | 8.0   | 18.4  | 49.0  | 0.0   | 0.0   |
| 3     | 8.0   | 7.2   | 14.6  | 46.6  | 0.0   | 0.0   |
| 4     | 9.0   | 6.0   | 14.4  | 46.0  | 0.0   | 0.0   |
| 5     | 7.6   | 7.4   | 14.0  | 43.0  | 0.0   | 0.0   |
| 6     | 9.8   | 5.8   | 13.8  | 39.6  | 0.0   | 0.0   |
| 7     | 7.2   | 6.4   | 12.2  | 37.9  | 0.0   | 0.0   |
| 8     | 13.0  | 6.6   | 13.0  | 25.8  | 0.0   | 0.0   |
| 9     | 9.0   | 7.6   | 11.8  | 27.9  | 0.0   | 0.0   |
| 10    | 5.8   | 9.4   | 14.0  | 32.9  | 0.0   | 0.0   |
| 11    | 7.6   | 9.4   | 17.4  | 52.7  | 0.0   | 0.0   |
| 12    | 5.4   | 10.0  | 19.0  | 55.0  | 0.0   | 0.0   |

**Table A6:** M3 (Pause) linear probe accuracy (%), 5-fold CV).

## A.10 Nonlinear Probe Results

Our initial MLP probes (2-layer, 256 hidden units, scikit-learn MLPClassifier with default hyperparameters) pro-

| Layer | Pos 0 | Pos 1 | Pos 2 | Pos 3 | Pos 4 | Pos 5 |
|-------|-------|-------|-------|-------|-------|-------|
| 0     | 3.2   | 3.2   | 4.4   | 4.4   | 0.0   | 0.0   |
| 1     | 3.6   | 1.8   | 5.0   | 6.4   | 0.0   | 0.0   |
| 2     | 5.8   | 3.0   | 4.4   | 5.0   | 0.0   | 0.0   |
| 3     | 5.0   | 3.0   | 4.2   | 7.4   | 0.0   | 0.0   |
| 4     | 5.2   | 3.6   | 4.4   | 8.4   | 0.0   | 0.0   |
| 5     | 6.8   | 3.0   | 5.8   | 11.4  | 0.0   | 0.0   |
| 6     | 7.4   | 5.8   | 4.6   | 8.4   | 0.0   | 0.0   |
| 7     | 10.4  | 4.0   | 3.4   | 4.7   | 0.0   | 0.0   |
| 8     | 23.6  | 5.4   | 3.8   | 2.7   | 0.0   | 0.0   |
| 9     | 14.6  | 9.2   | 6.8   | 3.0   | 0.0   | 0.0   |
| 10    | 11.0  | 9.0   | 6.6   | 4.7   | 0.0   | 0.0   |
| 11    | 10.0  | 10.4  | 21.6  | 53.0  | 0.0   | 0.0   |
| 12    | 10.2  | 7.8   | 22.0  | 57.0  | 0.0   | 0.0   |

duced a uniform 0/78 null result. As anticipated, this reflected convergence failure rather than a genuine absence of nonlinear encoding.

**Grid search methodology.** We conducted a systematic hyperparameter search over the five cells with highest linear probe accuracy: M2 (layer 0, position 3), M2 (layer 12, position 2), M3 (layer 12, position 3), M3 (layer 8, position 0), and M3 (layer 12, position 2). For each cell, we evaluated 72 configurations: 6 hidden layer sizes (64, 96, 128, 192, 256, 512)  $\times$  3 learning rates (0.0001, 0.001, 0.01)  $\times$  4 L2 regularization strengths (0.0001, 0.001, 0.01, 0.1), using 5-fold cross-validation and `max_iter=2000`.

**Table A7:** MLP probe grid search results at five target cells (advantage = best MLP accuracy – linear probe accuracy).

| Model | Layer | Pos | N   | Linear | Best MLP | Advantage |
|-------|-------|-----|-----|--------|----------|-----------|
| M2    | 0     | 3   | 298 | 55.4%  | 46.0%    | -9.4pp    |
| M2    | 12    | 2   | 500 | 19.0%  | 29.2%    | +10.2pp   |
| M3    | 12    | 3   | 298 | 57.0%  | 45.6%    | -11.4pp   |
| M3    | 8     | 0   | 500 | 23.6%  | 14.6%    | -9.0pp    |
| M3    | 12    | 2   | 500 | 22.0%  | 29.6%    | +7.6pp    |

At **position 3** (the answer hop), linear probes outperform MLPs by approximately 10 percentage points. Two non-exclusive factors likely contribute: (1) with  $n = 298$  samples and 38 target classes (~7.8 samples per class), the MLP’s larger parameter count overfits despite regularization; and (2) since the answer-generation head is itself a linear projection, training may explicitly produce a linearly separable representation at this position — a format that linear probes recover by design but that additional nonlinear capacity cannot exploit further.

At **position 2** (the intermediate hop), MLPs show a substantial advantage: +10.2 percentage points for M2 and +7.6 for M3. With  $n = 500$ , overfitting is less severe, and

the MLP captures nonlinear structure that linear probes miss. This suggests that intermediate reasoning steps are encoded in a more complex, nonlinearly distributed format, while the final answer is projected into a linearly decodable subspace.

Both models show the same qualitative pattern (linear-sufficient at position 3, nonlinear advantage at position 2), consistent with the shared curriculum producing similar representational strategies.

### A.11 Full Probing Heatmaps and Additional Analysis

**Probing heatmaps.** Figure 5 shows the full linear probe accuracy heatmaps across all layers and thought positions for both models.

*Figure reproduced in Section 4.3.*

The two models concentrate decodable information at different locations in the network. M2’s peak probe accuracy occurs at layer 0, position 3. Because COCONUT recycles the final-layer hidden state back into the input embedding stream, the recycled representation arrives pre-processed at layer 0, making intermediate information linearly accessible from the earliest layer. M3 builds its representations through the transformer stack, with peak accuracy at layer 12 (the final layer). The diagonal peak layers for M2 are [8, 12, 12, 0] across positions 0–3; for M3 they are [8, 11, 12, 12]. These patterns reflect architectural differences in where information is injected, not differences in what information is encoded.

**Thought-vs-input advantage.** M2’s thought-token positions encode 10.5% more decodable information than its input positions, compared with 4.0% for M3. The recycling mechanism creates broadly distributed, robustly decodable intermediate representations, consistent with its architectural design. But this richer encoding does not produce a different selectivity pattern, a binary-accuracy advantage, or a change in OOD generalization direction — though it does produce measurably higher per-sample confidence (Section 4.5).

**Layer-dependent selectivity for M3.** Table 3 reports selectivity at layer 12 for all M3 positions. At alternative layers, selectivity values differ: position 0 shows +17.0pp (positive, not anti-selective) at layer 8, while position 1 shows -11.2pp at layer 11. The anti-selectivity pattern at early positions is thus layer-dependent for M3.

### A.12 M2 vs. M3 Pairwise OOD Comparisons

This table is retained from the two-model analysis for completeness. The M2 vs. M3 comparison is confounded by the forward-pass asymmetry; the factorial decomposition (Table 5) provides the clean attribution.

**Table A8:** Pairwise McNemar comparisons (M3 vs. M2).

| Test Set    | M3 – M2 | b   | c   | p (exact) | p (Bonf.) | Sig. |
|-------------|---------|-----|-----|-----------|-----------|------|
| ProsQA (ID) | -0.4 pp | 12  | 14  | 0.845     | 1.000     | No   |
| 7-hop       | +9.4 pp | 214 | 120 | < 0.001   | < 0.001   | Yes  |
| 8-hop       | +7.6 pp | 198 | 122 | < 0.001   | < 0.001   | Yes  |
| DAG         | -7.3 pp | 162 | 235 | < 0.001   | 0.0015    | Yes  |
| Dense       | +7.2 pp | 211 | 139 | < 0.001   | < 0.001   | Yes  |

### A.13 Full Convergent Evidence Table

Section 5.1 in the main text provides a compact summary. Table A9 below gives the full analysis with detailed discussion of each diagnostic.

**Table A9:** Full convergent evidence across experimental paradigms with detailed results.

**Additivity analysis.** The decomposition is approximately additive: on 7-hop, the recycled-content penalty (10.9pp) plus the neutral sequential-processing effect (1.5pp, ns) approximates the M3–M2 difference (9.4pp); on DAG, the sequential-processing advantage (7.9pp) plus the neutral recycled-content effect (0.6pp, ns) approximates the M2–M3 difference (7.3pp). On dense graphs, the recycled-content penalty (+3.6pp, ns) and the sequential-processing penalty (-3.6pp, ns) cancel additively, producing a near-zero net difference that masks opposing underlying forces rather than indicating an interaction.

**Detailed discussion.** No single experiment is decisive in isolation. Permutation insensitivity could in principle reflect redundant encoding, where each position stores a complete copy of the reasoning chain. However, single-position corruption rules this out: if all positions stored the complete chain redundantly, corrupting any single position should be compensated by the remaining uncorrupted copies. Instead, corrupting position 3 alone collapses accuracy to ~57% (Table A4), indicating that critical information is concentrated at position 3 rather than redundantly distributed. Cross-transplant tolerance could indicate overlapping representations. But taken together, seven independent diagnostics consistently fail to find evidence that COCONUT’s recycled hidden states carry reasoning content that differs functionally from M3’s learned pause vectors on in-distribution evaluation. The convergence across methods strengthens the conclusion beyond what any single test provides.

The OOD results add nuance: M2 and M3 show a task-dependent generalization tradeoff, which M4’s factorial decomposition fully resolves — attributing M2’s chain-length disadvantage to recycled content and M2’s DAG advantage to sequential processing. The teacher-forced confidence analysis adds a further dimension: M2’s re-

| Evidence                |                           | Sequential reasoning prediction  | Curriculum-driven prediction  | Our result |
|-------------------------|---------------------------|----------------------------------|---|------------|
| Permutation sensitivity | Order matters             | Order irrelevant (for output)    | 0% flip rate for both M2 and M3   |            |
| Cross-transplant        | Problem-specific states   | Generic / curriculum-shaped      | Both tolerate foreign thoughts (M2: 97.0%, M3: 96.5%); unmatched pairing equally effective  |            |
| Corruption cliff        | Gradual cascade           | Threshold collapse               | Identical cliff at position 4 for both models; persists under 50× noise scaling   |            |
| Probing selectivity     | M2-specific step encoding | Shared curriculum-driven pattern | Both models show identical selectivity profiles: strong step-specificity at position 3 (+52pp), anti-selectivity at positions 0–1, arising from shared curriculum |            |
| Probing significance    | M2 broadly significant    | Equal significance               | M2: 29/78 significant cells; M3:  |            |

cycled content produces significantly higher per-sample confidence on in-distribution data, confirming that the recycled hidden states carry reasoning-relevant information. However, this higher confidence becomes miscalibrated on OOD chain-length tasks, where M2 is simultaneously more confident and less accurate than M4.

## A.14 Wilcoxon Confidence Tables

**Table 6a:** Clean comparison — recycled content (M2 vs. M4). Wilcoxon signed-rank on teacher-forced species-token log-probabilities.  $r$  = rank-biserial correlation. Bonferroni-corrected ( $k = 5$ ). Both models share sequential processing; the comparison isolates the effect of recycled content.

| Test Set    | n    | r     | p (Bonf.)    | Direction | Sig. |
|-------------|------|-------|--------------|-----------|------|
| ProsQA (ID) | 500  | 0.678 | $< 10^{-50}$ | M2 > M4   | Yes  |
| 7-hop       | 1000 | 0.109 | 0.003        | M2 > M4   | Yes  |
| 8-hop       | 1000 | 0.082 | 0.049        | M2 > M4   | Yes  |
| DAG         | 1000 | 0.073 | 0.106        | —         | No   |
| Dense       | 1000 | 0.118 | 0.001        | M2 > M4   | Yes  |

**Table 6b:** Confounded comparison — forward-pass asymmetry (M2 vs. M3). M2 processes sequentially, M3 in parallel; interpret through the factorial decomposition.

| Test Set    | n    | r     | p (Bonf.)    | Direction | Sig. |
|-------------|------|-------|--------------|-----------|------|
| ProsQA (ID) | 500  | 0.591 | $< 10^{-38}$ | M2 > M3   | Yes  |
| 7-hop       | 1000 | 0.006 | 1.000        | —         | No   |
| 8-hop       | 1000 | 0.006 | 1.000        | —         | No   |
| DAG         | 1000 | 0.003 | 1.000        | —         | No   |
| Dense       | 1000 | 0.113 | 0.002        | M3 > M2   | Yes  |

**Confounded comparison (M2 vs. M3).** The M2 vs. M3 comparison is confounded by the forward-pass asymmetry (Section 6) and is retained for completeness. M2 shows higher in-distribution confidence ( $r = 0.591$ ,  $p < 10^{-38}$ ) but no significant confidence difference on 7-hop or 8-hop ( $r < 0.01$ ,  $p = 1.0$ ), consistent with the chain-length tasks neutralizing the recycled-content signal.

## A.15 M3 vs. M4 Confidence Details

The M3 vs. M4 comparison reveals that sequential processing (controlling for content) increases OOD confidence.

**Table A10:** Wilcoxon signed-rank comparisons: M3 vs. M4. Bonferroni-corrected ( $k = 5$ ).

On ProsQA (in-distribution), M3 assigns higher median probabilities than M4 ( $r = 0.286$ ,  $p < 10^{-9}$ ), consistent with the single-pass architecture maintaining higher in-distribution confidence. On OOD test sets, M4 assigns higher median probabilities than M3 on 7-hop

| Comparison | Test Set    | n    | r     | p (Bonf.) | Direction | Sig. |
|------------|-------------|------|-------|-----------|-----------|------|
| M3 vs. M4  | ProsQA (ID) | 500  | 0.286 | < 10^{-9} | M3 > M4   | Yes  |
| M3 vs. M4  | 7-hop       | 1000 | 0.142 | < 0.001   | M4 > M3   | Yes  |
| M3 vs. M4  | 8-hop       | 1000 | 0.120 | 0.001     | M4 > M3   | Yes  |
| M3 vs. M4  | DAG         | 1000 | 0.136 | < 0.001   | M4 > M3   | Yes  |
| M3 vs. M4  | Dense       | 1000 | 0.021 | 1.000     | —         | No   |

( $r = 0.142$ ), 8-hop ( $r = 0.120$ ), and DAG ( $r = 0.136$ ), all significant. On DAG, this higher confidence aligns with M4’s higher accuracy (+7.9pp). On 7-hop and 8-hop, M4’s slightly higher accuracy (+1.5pp and +0.1pp, both ns by McNemar) is accompanied by significantly higher confidence, suggesting that sequential processing produces better-calibrated representations on OOD tasks — a benefit that is modest in accuracy terms but substantial in confidence terms.

## A.16 Detailed Limitation Analysis

**Scale.** All experiments use GPT-2 124M, a model with 12 layers and 768-dimensional hidden states. Zhang et al. (2025) conducted their causal intervention study on LLaMA 7B and 8B, which are 56–64 times larger. It is possible that the continuous thought mechanism provides benefits that emerge only at larger scale, where the model has sufficient capacity to learn the superposition states that Zhu et al. (2025) proved are theoretically available. Our negative results establish that the mechanism is not necessary for ProsQA performance at 124M parameters, but they do not rule out scale-dependent effects. Replication at LLaMA-class scale would substantially strengthen or weaken our claims.

**Task complexity.** ProsQA is a synthetic graph-traversal benchmark with perfectly structured, unambiguous reasoning paths. Each problem has a unique correct answer, the graph topology is fully specified, and there is no lexical or semantic ambiguity. Natural language reasoning involves noise, underspecification, conflicting evidence, and graded plausibility. The recycling mechanism’s ability to encode superposition states (Zhu et al., 2025) may be more valuable in settings where the model must maintain multiple candidate interpretations simultaneously — a capacity that ProsQA’s deterministic structure does not require. Our conclusions are specific to tasks with this structural profile.

**Single seed.** All results are from a single training seed (seed 0). The 0.4-percentage-point test-set gap between M2 (97.0%) and M3 (96.6%) is not statistically significant (McNemar  $p = 0.845$ ), but could widen or reverse under different random initializations. The out-of-distribution advantages we report for M3 — including the 9.4-point gap on 7-hop paths — may similarly reflect seed-specific training dynamics rather than systematic architectural differences. Replication across

3–5 training seeds with paired statistical tests would provide confidence intervals around these estimates and clarify whether M4’s 94.8% reflects a systematic gap or initialization variance; in particular, whether the robustness of ID equivalence versus the variability of OOD effects is itself seed-dependent remains untested. Training-time evaluation at best epoch yielded a larger apparent gap ( $M2 = 98.0\%$ ,  $M3 = 95.6\%$ ), differing from the experiment-pipeline numbers by 5 samples per model in opposite directions; this sensitivity to the inference code path underscores the need for multi-seed replication.

**Forward-pass asymmetry (addressed by M4).** M2 processes thought tokens sequentially via KV-cache incremental decoding, while M3 processes all thought tokens in a single forward pass. In the two-model comparison, this meant M2 and M3 differed in two confounded ways: (1) the content of thought-token embeddings and (2) the sequential processing structure. M4 resolves this confound by matching M2’s sequential processing while using M3’s fixed embeddings. While M4 resolves the content-vs-processing confound, a residual asymmetry remains: M4 and M2 process the same number of sequential steps, but the information available at each step differs qualitatively (fixed embedding vs. a representation that reflects accumulated state). This is an inherent property of the recycling mechanism and cannot be further decomposed without more invasive interventions.

**Curriculum isolation.** Our design controls for the continuous thought mechanism by replacing it with pause tokens while preserving the curriculum. However, we do not test a curriculum-only condition in which removed reasoning tokens are simply deleted, producing shorter sequences with no additional attention positions. We therefore cannot distinguish whether the curriculum alone drives the gains or whether the curriculum requires additional attention positions as a computational budget. A curriculum-only ablation would resolve this ambiguity.

**Probing measures presence, not use.** M2’s 10.5% mean thought-position advantage over input positions, and its nearly 3× greater number of significant probing cells (29/78 vs. 11/78), demonstrate that the recycling mechanism has a measurable and substantial effect on the model’s internal representations. The mechanism is not “doing nothing” — it injects broadly distributed, decodable information that the pause baseline does not contain. Our claim is narrower: this richer encoding does not produce a different representational strategy or an accuracy advantage. But the distinction between presence and use is subtle; a more sensitive behavioral measure

might reveal functional consequences. Additionally, probing results for thought positions 4 and 5 ( $n = 81$  and  $n = 12$ , respectively) have limited statistical power; our quantitative claims rest primarily on positions 0–3.

**Corruption noise calibration.** The per-model noise calibration produces substantially different absolute perturbation magnitudes ( $L_2 = 202.65$  for M2 vs. 4.09 for M3), reflecting the 50-fold variance difference between recycled hidden states and near-constant pause embeddings. Our cross-scale analysis (applying M2-magnitude noise to M3) confirms that the degradation cliff is structural rather than scale-dependent, but the quantitative degradation curves under per-model calibration are not directly comparable across models.

**M4 experimental coverage.** The corruption analysis and representational probing experiments could not be extended to M4 due to a methodological incompatibility with multi-pass KV-cache architectures (see Appendix A.1). Extending these experiments to M4 would require per-pass hidden state collection from within the KV-cache loop, which we leave for future work.

## A.17 OOD Dataset Statistics

All OOD test sets contain 1,000 samples generated using ProsQA’s vocabulary (38 species names, 17 person names) with seed 42.

**Table A11:** OOD dataset generation parameters.

| Test Set    | n    | Path Length | Graph Type | Branching Factor |
|-------------|------|-------------|------------|------------------|
| ProsQA (ID) | 500  | 3–6         | Tree       | 2–4              |
| 7-hop       | 1000 | 7           | Tree       | 2–4              |
| 8-hop       | 1000 | 8           | Tree       | 2–4              |
| DAG         | 1000 | 3–6         | DAG        | 2–4              |
| Dense       | 1000 | 3–6         | Tree       | 5–8              |

## A.18 Datasets

**Examples** We provide an example of the questions and chain-of-thought solutions for ProsQA.

**Question:** “Every shumpus is a rempus. Every shumpus is a yimpus. Every terpus is a fompus. Every terpus is a gerpus. Every gerpus is a brimpus. Alex is a rempus. Every rorpus is a scrompus. Every rorpus is a yimpus. Every terpus is a brimpus. Every brimpus is a lempus. Tom is a terpus. Every shumpus is a timpus. Every yimpus is a boompus. Davis is a shumpus. Every gerpus is a lorpus. Davis is a fompus. Every shumpus is a boompus. Every shumpus is a rorpus. Every terpus is a lorpus. Every boompus is a timpus. Every fompus is a yerpus. Tom is a dumpus. Every rempus is a rorpus. Is Tom a lempus or scrompus?”

**Reasoning steps:** [“Tom is a terpus.”, “Every terpus is a brimpus.”, “Every brimpus is a lempus.”]

**Answer:** “Tom is a lempus.”

The input contains 23 statements, of which only 3 are relevant to the answer. The remaining 20 are valid inheritance rules involving other entities (Alex, Davis) and concept chains that serve as distractors.

**Construction of ProsQA** ProsQA is constructed following the methodology of Hao et al. (2024), which draws on the entity-concept naming conventions of ProntoQA (Saparov and He, 2022). Each problem is structured as a binary question: “Is [Entity] a [Concept A] or [Concept B]?” where [Concept A] is the correct answer.

The underlying graph is a directed acyclic graph (DAG) where each node represents an entity or a concept. The graph is constructed such that a path exists from [Entity] to [Concept A] but not to [Concept B]. New nodes are incrementally added and randomly connected with edges. With probability 0.35, the new node is constrained to not be a descendant of node 1 (the correct-answer branch); with probability 0.35, it is constrained to not be a descendant of node 0 (the entity); otherwise, it may connect to any existing node. This separation maintains distinct families of nodes and balances their sizes to prevent model shortcuts. Sampling weights prioritize deeper nodes ( $\text{weight} = \text{depth} \times 1.5 + 1$ ) to encourage longer reasoning chains. The number of incoming edges per new node is drawn from Poisson(1.5).

After graph construction, root nodes (those without parents) are assigned entity names (e.g., “Tom,” “Alex”), while other nodes receive fictional concept names (e.g., “brimpus,” “lorpus”). Node 0 becomes the queried [Entity], a leaf labeled 1 becomes [Concept A], and a leaf labeled 2 becomes [Concept B]. The two answer options are randomly permuted to avoid positional biases.

**Table A12:** Statistics of the ProsQA graph structure (from Hao et al., 2024).

| # Nodes | # Edges | Len. of Shortest Path | # Shortest Paths |
|---------|---------|-----------------------|------------------|
| 23.0    | 36.0    | 3.8                   | 1.6              |

**Table A13:** Dataset split sizes.

| Dataset | Training | Validation | Test |
|---------|----------|------------|------|
| ProsQA  | 17,886   | 300        | 500  |